AFOSR-TR-97-0370

REPORT DOCUMENTATION PAGE

Form Approved
OMB No. 0704-0188

1. AGENCY USE ONLY (Leave blank)	2. REPORT DATE	3. REPORT TYPE AND DATES COVERED
	19 Feb 1997	Final 1 Dec 1993 - 30 Nov 1996

4. TITLE AND SUBTITLE
Modes, rays and scattering: A Basic Study of Seismic Wave Propagation at Regional Distances

5. FUNDING NUMBERS
PE 61102F
Proj 2309/AS
F49620-94-1-0077

6. AUTHOR(S)
Guust Nolet
F.A. Dahlen
R.A. Phinney

7. PERFORMING ORGANIZATION NAME(S) AND ADDRESS(ES)
Department of Geological & Geophysical Sciences
Princeton University
Princeton NJ 08544

8. PERFORMING ORGANIZATION REPORT NUMBER
No number

9. SPONSORING MONITORING AGENCY NAME(S) AND ADDRESS(ES)
AFOSR/NM
110 Duncan Ave
Bolling AFB DC 20332

10. SPONSORING/MONITORING AGENCY REPORT NUMBER
Monograph Series of Seismic Research #97-04

11. SUPPLEMENTARY NOTES

12a. DISTRIBUTION AVAILABILITY STATEMENT

APPROVED FOR PUBLIC RELEASE:
DISTRIBUTION UNLIMITED

19971003 050

13. ABSTRACT (Maximum 200 words)

The objective of this research was to systematically explore the attributes of the wave form Lg and related wave forms which are trapped in the crust. The different theoretical approximations used to characterize or to fully compute regional seismic waves were thoroughly investigated. Empirical classification of the behavior of Lg was achieved through waveform data analyses. The Kennett conjecture that Lg waves can be adequately described by multiple S energy trapped in the crust has been adopted. It has been shown that Lg magnitudes are much more stable than the chaotic behavior of the ray would seem to imply. As a result of recognizing that a large number of caustic are generated as a consequence of the chaotic ray beharior, it was decided that Maslov theory was probably the only suitable technique to deal with the singularity problem. As a result, it has been shown that Maslov synthetics can be used to justify the use of ray density plots as energy plots, which can be used in turn for the calibration of Lg magnitudes. The 3-component array and single station data from the NPE 1993 detonation have been analyzed in order to examine the effects boundary undulations of the crustal wave guide may have on propagation.

14. SUBJECT TERMS	15. NUMBER OF PAGES
Seismology Propagation of Lg Regional seismic detection	30
	16. PRICE CODE

17. SECURITY CLASSIFICATION OF REPORT	18. SECURITY CLASSIFICATION OF THIS PAGE	19. SECURITY CLASSIFICATION OF ABSTRACT	20. LIMITATION OF ABSTRACT
UNCLASSIFIED	UNCLASSIFIED	UNCLASSIFIED	SAR

AFOSR F49620-94-1-0077: Modes, rays and scattering: a basic study of seismic wave propagation at regional distances.

Final Technical Report

G. Nolet (PI), F.A. Dahlen (Co-PI), R.A. Phinney (Co-PI)

Department of Geological and Geophysical Sci., Princeton University, Princeton, NJ 08544

Our project aimed for a systematic exploration of the attributes of Lg and related trapped waves in the crust. We studied the different theoretical approximations used to characterize or fully compute regional seismic waves, and analyzed waveform data to develop an empirical classification of the behaviour of Lg.

From the beginning we adopted Kennett's conjecture that Lg waves could be adequately described by multiple S energy trapped in the crust. We developed software to generate synthetics by ray summation and validated this against a mode-summation code for horizontally layered models [1-4,7,14]. We then set out to perturb the depth to the Moho to obtain more realistic, complicated seismograms [12]. When we discovered that the chaotic nature of the kinematics of the trapped rays is a major characteristic of Lg waves [5,8], we judged this discovery important enough to warrant extra attention. In a first application, we showed that Lg magnitudes are much more stable measurements than the chaotic behaviour of the ray would led one to expect [5,11]

One consequence of the chaotic ray behavior is the large number of caustics that are generated. These, in turn, lead to singularities that render the more common ray summation techniques useless. We decided that Maslov theory was probably the only suitable technique to deal with the singularity problem [6], and set out to compute the correct Maslov phase and amplitude using the method of stationary phase. We called in the help of Chris Chapman at

Schlumberger (UK), and Henk Keers spent the summer of 1995 working with him in Cambridge to solve the problems posed by pseudo-caustics in calculating Maslov synthetics (pseudo caustics are essentially plane wave arrivals that often accompany regular caustic singularities) [6,10,11].

An algorithm is ready that efficiently computes 2D Maslov integrals. This algorithm is essential for the fast computation of synthetics in 3D heterogeneous media. The latter development is still in progress, and will form the concluding chapter of Keers' PhD thesis. Very complete seismograms can be generated in crustal models of arbitrary complexity through the generation of multiples, for which we developed an efficient tree algorithm [8].

In a parallel observational study, we made sure that our theoretical foundations where always strongly based on the reality of regional seismograms. This part of the project was carried by Kristin Vogfjörd. She analyzed 3-component array- and single-station data, recording the NPE explosion in 1993, on a profile extending from the NTS, westward across the Sierra Mountains [18, 21, 23]. P_mP and S_mS are coherent into the Sierras, but disappear due to the crustal gradient at around 230 km distance. They arrive off-azimuth indicating a dip on the Moho at the reflection. The second multiple Moho reflections are not so clearly observed. Due to the Moho undulations the rays in the second Moho multiple start to diverge and are not clearly traced into the Sierras. Only one of the arrays has coherent arrivals corresponding, in time and phase velocity, to $2P_mP$ and $2S_mS$. This confirmed our theoretical findings that, while multiple S is important in building up the Lg wavetrain, internal multiples and crustal heterogeneity are important and must be coinsidered when explaining Lg and its characteristics.

The observation that S is important even in explosively generated waves requires a theoretical understanding. In the literature, there is no consensus on this topic. Vogfjörd established that explosions can generate sufficient S^* energy to allow for the validity of Kennett's hypothesis [13,15,16,24]. Vogfjörd examined effects of two parameters, source depth and Moho undulations, on the development and character of the crustal wave trains (P, L_g). If source depth is within 1 km from the surface, and the velocity structure is such that the peak in the S^* radiation pattern is trapped in the crust, then S^* contributes significantly to L_g. However if the source radiates shear waves, includes spall, or tectonic release this contribution may be drowned in the

S waves emanating from these other terms. Explosion sources that do not include any significant amount of these contributing factors, on the other hand, may lead to S^* dominated L_g wave trains. Such sources are possibly representative of decoupled nuclear explosions, as well as some singe-shot underground mining explosions. Since decoupled nuclear explosions represent a plausible threat to a comprehensive test ban, observations of S^* signature in L_g could possibly be an important discriminant of such evasive testing [17,19,24].

The importance of the depth parameter for discrimination led to a second study on $2P_g$ in the crustal P wave train and $2S_g$ in the L_g wave train, using data from the Iceland SIL network [16, 20, 22]. Their relative arrival-time is strongly depth dependent and thus provides a fixed constraint on the depth of shallow sources. The results have been reported in [16], and a paper is in preparation [22].

The Maslov synthetics can be used to justify the use of ray density plots as energy plots, which can be used in turn for the calibration of Lg magnitudes. In order to examine the effects that undulations on the boundaries of the crustal wave-guide have on the propagation of crustal wave trains, we analyzed the 3-component array- and single-station data from the NPE explosion in 1993. A paper detailing the results is in preparation [23].

References

1. Das, T. and G. Nolet, Crustal thickness estimation using high frequency Rayleigh waves, *Geophys. Res. Lett.*, **22**, 539-542, 1995.

2. Keers, H. and G. Nolet, Lg-wave propagation using mode and ray summation, EOS, Transactions AGU, Spring Meeting suppl., 227, 1994.

3. Keers, H. K. Vogfjord, G. Nolet and R. Phinney, Lg synthesis in media with undulating surfaces by ray summation, EOS, Transactions AGU, Fall Meeting suppl., 420, 1994.

4. Keers, H., K. Vogfjord, G. Nolet and R. Phinney, Lg waves by ray and mode summation; a first comparison, Abstracts of the 16th annual seismic research symposium of AFOSR, p. 27, 1994

5. Keers, H., G. Nolet and F.A. Dahlen, Chaos and Lg waves, EOS Trans. AGU, Spring Meeting suppl., S204, 1995.

6. Keers, H., Nolet G., and Dahlen F. A., Wave Chaos and Maslov Integrals, EOS, **77**, 178, 1996.

7. Keers, H., Nolet G., and Dahlen F. A., Ray Theoretical Analysis of Lg, *Bull. Seism. Soc. Am.*, **86**, 726-736, 1996.

8. Keers, H., Dahlen F. A., and Nolet G., Chaotic Ray Behavior in Seismology, *Geoph. Journal. Int.*, submitted, 1996.

9. Keers. H., Nolet G., and Dahlen F. A., Crustal Wave Propagation in California, EOS, **77**, 524, 1996.

10. Keers. H., and Chapman C. H., Maslov Theory and Pseudo-caustics (in preparation), 1997.

11. Keers. H., G. Nolet and F.A. Dahlen, The computation of ampltude envelopes in strongly heterogeneous media; theory and applications, EOS 77, Fall Meeting Suppl., F524, 1996.

12. Vogfjord. K., G. Nolet, R. Phinney and A. Dahlen, An attempt at modelling Lg in complex media. EOS. Transactions AGU, Fall Meeting suppl., 419, 1994.

13. Vogfjord. K., G. Nolet F.A. Dahlen, Excitation of Lg from shallow sources. EOS, Transactions AGU. Spring Meeting suppl., 1994.

14. Vogfjord. K., H. Keers. G. Nolet, F.A. Dahlen and R. Phinney, Composition of Lg, NATO Advanced Study Institute on Monitoring a Comprehensive Test Ban Treaty, Alvor Portugal, 23 Jan - 2 Feb, 1995.

15. Vogfjord, K., G. Nolet and F.A. Dahlen, Excitation of Lg from shallow sources, EOS Trans. AGU, Spring Meeting suppl., S204, 1995.

16. Vogfjord K.S. , Depth phases in SIL seismograms from local earthquakes, ESC Meeting, Reykjavik, 1996.

17. Vogfjord, K.S., G. Nolet and F.A. Dahlen, Regional characterization of crustal wavetrains, a prerequisite for reliable regional discrimination, ESC Meeting, Reykjavik, 1996.

18. Vogfjord, K., G. Nolet, R. Phinney and F.A. Dahlen, Propagation of crustal wavetrains accross the Sierra Nevada, EOS 77, Fall Meeting Suppl., F14, 1996.

19. Vogfjörd, K. S., G. Nolet, and A. F. Dahlen, Regional characterization of crustal wave trains. A prerequisite for reliable regional discrimination, *European Seismological Commission, XXV General Assembly*, 132, 1996.

20. Vogfjörd, K. S., Depth phases in SIL seismograms from local earthquakes. *European Seismological Commission, XXV General Assembly*, 74, 1996.

21. Vogfjörd, K. S., G. Nolet, R. P. Phinney and A. F. Dahlen, Propagation of crustal wave trains across the Sierra Nevada, *EOS*, **77**, No 46, 1996.

22. Vogfjörd, K. S., Depth phases in local earthquake data from the SIL network in Iceland, (in preparation), 1997.

23. Vogfjörd, K. S., H. Keers, G. Nolet, R. P. Phinney and A. F. Dahlen, Effects of Moho undulations on the propagation of crustal wave trains (in preparation), 1997.

24. Vogfjörd, K. S., Effects of explosion depth and Earth structure on excitation of Lg: S^* revisited, in press, *Bull. Seism. Soc. Am.*, 1997.

The Character of Lg-Waves from a Mode and Ray Point of View

H. Keers, K. Vogfjörd, G. Nolet, R. Phinney

Department of Geological and Geophysical Sciences
Princeton University
Princeton, NJ 08544

Contract number: F49620-94-1-0077

OBJECTIVE

The objective of our research is to find ways to compute synthetics of Lg-waves in complicated heterogeneous media. Lg-waves are the most prominent phases on regional seismograms. As such they are important in studying seismic sources and the structure of the crust and upper mantle.

In our study we look at Lg-waves from both a mode and a ray point of view (Kennett, 1986). The validation of the ray methods, by comparing them to the mode sum is the primary reason for this study. Both methods have been among the most successful in computing synthetics in heterogeneous media. However the ray method tends to be less difficult from a computational point of view.

To gain physical understanding we start by considering the propagation of Lg-waves in a simple layer over a halfspace. A comparison of the seismograms, computed using the two different methods is presented and an interpretation of the Lg-waves in terms of modes and rays is given. Subsequently we discuss the effects of an undulating Moho on the wave propagation; in doing so we emphasize ray theory, because of its computational advantages over mode theory. First we discuss one-point ray tracing and point out the limitations of two-point ray tracing. Because of the limitations of classical ray theory we also study the application of graph theory to this kind of models.

RESEARCH ACCOMPLISHED

Lg-waves in simple layered media

In order to understand the ray-mode duality of Lg-waves in layered media we take a simple layer over a halfspace model, see table 1. The source that we use is a strike-slip point source, at 8 km depth. All seismograms are calculated for points on a line through the source, perpendicular to the strike direction. For this preliminary investigation we only study SH waves. The calculated synthetics are all convolved with the WWSSN short period instrument response, which acts as a passband with corner frequencies of 1Hz and 3Hz.

Modes - Using the locked mode approximation of normal mode theory, synthetics have been calculated. The epicentral distance was 500 km. Figure 1 shows seismograms in which the first ten, twenty, forty and hundred modes are used. After comparing the seismograms we

conclude that ten modes are clearly not enough to model the whole Lg wavetrain. If twenty modes are used then the first half of the seismogram is reasonably well modelled, when compared with the seismogram in which hundred modes have been used. If forty modes are used then the result is quite satisfactory; except for the fact that the last part of the seismogram is not well modelled. It appears that we need around sixty additional modes in order to get one more arrival.

The latest arriving energy of each mode corresponds with the Airy phase. Even though the Airy phases are associated with a concentration of energy, they are not visible on the seismograms as separate arrivals, as suggested for example by Kovach and Anderson (1964). Rather, the formation of the different multiples is a consequence of a more complex superposition of the various modes.

Rays - In a simple layer over halfspace model it is easy to calculate all the ray paths from the source to the receiver, as well as the traveltimes and amplitudes of each ray. The amplitudes depend on the radiation pattern of the source, the pathlength of the ray and the reflection coefficient of the Moho. Using these quantities ray synthetics can readily be computed. An example of such synthetics are shown in figures 2 and 3. The only rays that contribute significantly to the seismogram are the super-critically reflected rays. In this case (epicentral distance of 500 km) there are twenty-one super-critical reflected rays. The twenty-second multiple has an amplitude that is a factor of 0.7×10^{-4} smaller than the twenty-first multiple, due to leakage of energy into the mantle. All super-critical reflected rays are clearly visible as separate arrivals, providing a simple interpretation of the seismogram in terms of rays. Because the reflection coefficient is complex the multiples have different phases. It should be noted that head-wave energy is not modelled with this method.

Mode-Ray duality - In figure 2 the mode and ray seismograms for different epicentral distances are presented. The overall agreement between the two methods is very good. In figure 3 blow-ups of the seismograms for an epicentral distance of five hundred kilometers are given. It appears that there are two major differences: the first difference is the presence of energy in the mode synthetic between the multiples. This is for instance visible in figure 3c, between 166s and 168s, and between 169s and 171s. This energy is not present in the ray synthetics. The second difference is the last multiple. This multiple is not present in the mode summation. Currently we believe that the energy in between the multiples is associated with (multiple) head-waves. Head-wave and multiple head-wave arrivals are not accounted for. The second discrepancy can be explained either by the incompleteness of the mode sum, such that more than 100 modes need to be taken into account, or by the failure of ray theory for rays reflected near critical angles.

It should be noted that in more complicated layered media not all ray arrivals are visible as separate arrivals, thus making the interpretation of the seismogram in terms of rays more complicated.

Lg-waves in simple heterogeneous media

As a next step we study the behavior of Lg-waves in a layer over a halfspace model with

an undulating Moho. From a modal point of view, in the high frequency approximation the waveforms should be identical to the model with a flat Moho and a crustal thickness equal to the average crustal thickness between source and receiver. If the high frequency approximation is not made, then the modes couple and the computation of synthetics becomes more difficult (Maupin, 1990).

Rays - From a ray point of view the first thing to do is one-point ray tracing. The situation is sketched in figure 4. The Moho is described by a given function f. The thickness of the crust at the horizontal coordinate x is given by $h + f(x)$. If, after n reflections the horizontal coordinate of the ray is x_n then after $n+1$ reflections the horizontal coordinate of the ray is given by

$$x_{n+1} = \psi_n + [h + f(\psi_n)] / \tan \theta_{n+1} \tag{1}$$

where ψ_{n+1} and θ_{n+1} are given by

$$\psi_n = x_n + [h + f(\psi_n)] / \tan \theta_n \tag{2}$$

and

$$\theta_{n+1} = \theta_n - 2 \arctan f'(\psi_n). \tag{3}$$

Note that these formulas hold if $x_n < \psi_n < x_{n+1}$. Similar formulas can be derived if x_n, ψ_n and x_{n+1} are permuted. It can be shown that $(x_n, \cos \theta_n)$ are canonically conjugate coordinates, i.e. the one-point ray tracing system can be written in terms of a Hamiltonian system.

For simplicity we took a simple sinusoid for f, with a wavelength of 100 km and an amplitude of 0.1 km. The average thickness is 20 km, the same as used in the layer over halfspace model. Figure 5 shows the results of the one-point ray tracing for SmS through $7\times SmS$. For SmS the first multipathing occurs for epicentral distances of 400 km.

For epicentral distances of 800 km and larger it becomes hard to do two-point ray tracing for SmS. If the undulation of the Moho becomes larger, then it turns out that it is hard to do any two-point ray tracing, and in fact the ray behavior is chaotic.

Graph-theoretical Rays - Because of these difficulties with two-point ray tracing in media with curved interfaces, it is worthwhile to investigate the possibility to use other methods, such as graph theory. Graph theory enables fast calculation of raypaths and travel times in complicated media, avoiding the problems mentioned above, and makes first order scattering computation possible. The method entails approximating ray paths with shortest-time paths between nodes in a grid and using Dijkstra's algorithm (Dijkstra, 1959) to search over all permissible raypaths between a source and a receiver. The search is made more efficient, by applying a sorting algorithm (Moser, 1991), making computation-time proportional to $n \log n$, where n is the number of nodes in the model.

The method finds only the shortest-time path; ray paths representing later arrivals can however be found by formulating them as constrained shortest paths. Scattered ray-paths

can be found by requiring the rays to visit a set of nodes. Moho reflections can also be obtained by stacking duplicates of the crust, the number of duplicates depending on the number of Moho reflections desired. For example, to obtain ray paths and travel times for SmS one duplicate of the crust is required, whereas for $2\times SmS$ a quadruplicated stack is needed. For one reflection the model consists of three interfaces: surface, Moho and surface. The source is located at a node on the surface, on one side of the model and the shortest-time ray paths are found to the nodes on the other surface, requiring the paths to go through the nodes on the intermediate interface, representing the Moho. We have made such an adaptation of the method, to obtain first arrivals for multiple Moho reflections of SH waves. Our initial model is the same as before. The nodes are 1 km apart on each copy of the Earth's surface and the Moho. To limit the ray paths to Moho reflections, nodes on one interface are only connected to nodes on the next one.

Ray paths of SmS first-arrivals in this model are shown in Figure 6. As distance increases beyond 140 km, the bounce-points of the first-arriving rays center around the peaks on the Moho, with fewer and fewer rays leaving the source ending up as first arrivals. Thus only a fraction of the energy leaving the source is present in these first arrivals. As the number of Moho multiples increases, even less of the source's energy is present in the first arrivals. Except for the reflection from each Moho peak, the first arrivals in this model are not geometric rays, as the reflection angles from the Moho deviate up to 0.07 deg from Snell's law, but rather represent diffracted waves from the peaks on the undulating Moho. Travel-time deviations from those of a flat Moho, are extremely small, due to the small amplitude of the Moho perturbation. Therefore, although the triplications produced by the sinusoidal Moho are not obtained with this method, the travel-time curve is nearly identical to the one obtained with the normal ray tracing method.

CONCLUSIONS AND RECOMMENDATIONS

We have come to a good understanding of Lg-waves from both a mode and a ray point of view in a simple layer over halfspace model, with a flat discontinuity. From a mode point of view the seismogram consists of the superposition of all modes. An interpretation in terms of Airy phases does not appear to be useful. From a ray point of view the seismogram consists of all crustal multiples that are critically reflected. The agreement between the seismograms obtained using these two methods is striking. The main difference is that head-waves are not modelled by the ray method in plane layered media.

If the Moho is undulating then the two-point ray tracing becomes much more complicated. It is nevertheless possible to do two-point ray tracing as long as neither the amplitude of the undulation nor the epicentral distance are too large. The graph theoretical traveltime results are nearly identical to those obtained with normal ray theory, thus providing a promising application of graph theory.

Further research should focus on the calculation of seismograms in media with one or possibly more curved interfaces. The possibilities and limitations of classical ray theory should be investigated, as well as the supplementary role that graph theory can play. It is also

necessary to compute seismograms in more complicated layered media, using both methods. As a next step P-SV waves need to be considered.

REFERENCES

Dijkstra, E. W., 1959. A note on two problems in connection with graphs. *Numer. Math.*, 1, 269-271.

Kennett, B. L. N., 1986. Lg waves and structural boundaries. *Bull. seism. Soc. Am.*, **76**, 1133-1141

Kovach, R. L. and Anderson, D. L., 1964. Higher mode surface waves and their bearing on the structure of the Earth's mantle, *Bull. seism. Soc. Am.*, **54**, 161-182.

Maupin, V., 1992. Modelling of laterally trapped surface waves with application to Rayleigh waves in the Hawaiian swell, *Geoph. J. Int.*, **110**, 553-570.

Moser, T. J., 1991. Shortest path calculation of seismic rays, *Geophysics*, **56**, 59-67.

Table 1	layer #	thickness (km)	S-velocity (km/s)	density (g/cm3)
	1	20	3.5	2.7
	2	2000	4.6	3.3
	3	inf	1000	1000

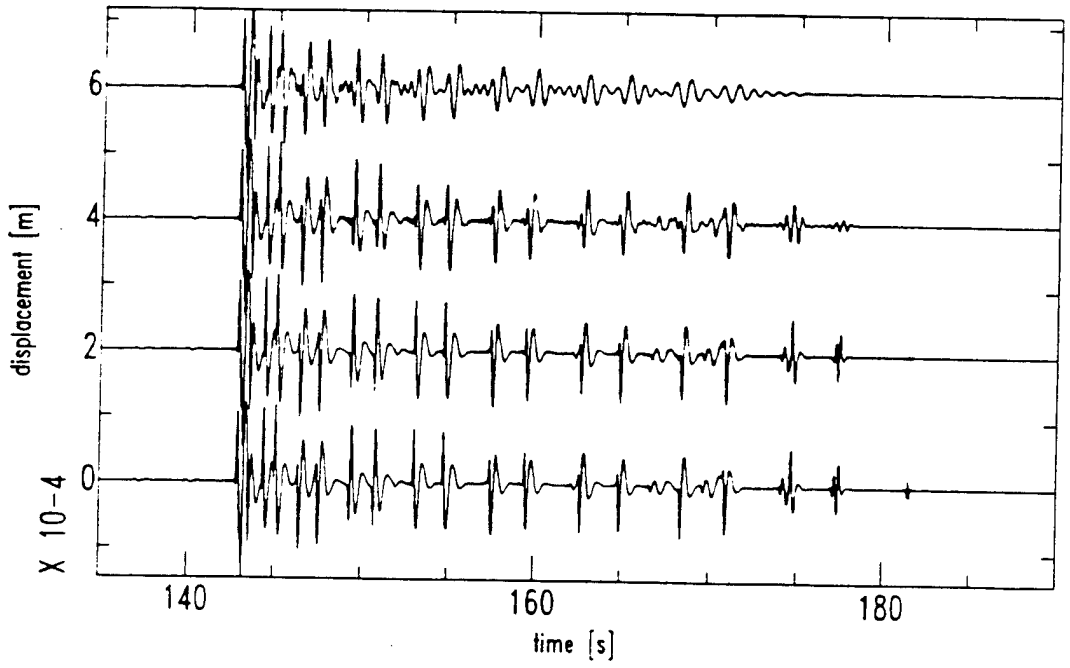

Figure 1. Mode-seismograms using (from top to bottom) 10, 20, 40 and 100 modes. The epicentral distance is 500 km.

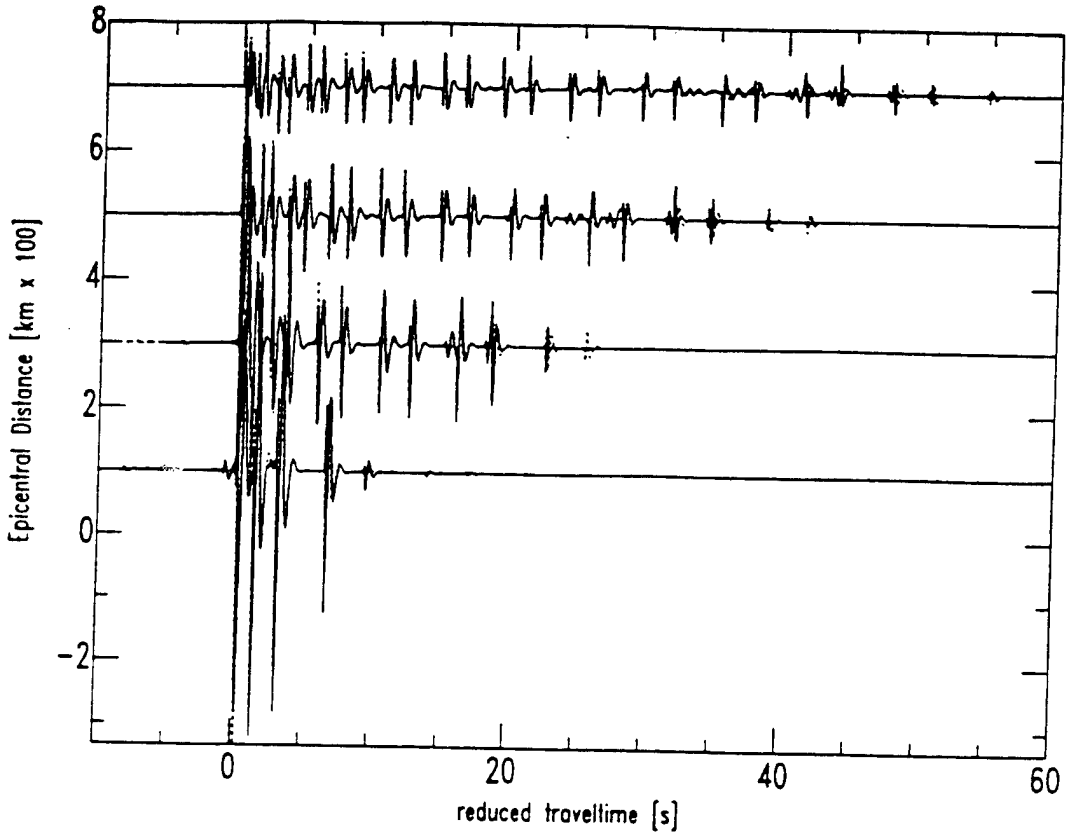

Figure 2. Comparison between seismograms computed using mode theory (solid) and ray theory (dashed). Epicentral distances are 100 km (bottom), 300 km, 500 km and 700 km (top). The reduced velocity is the S-wave velocity of the crust (3.5 km/s).

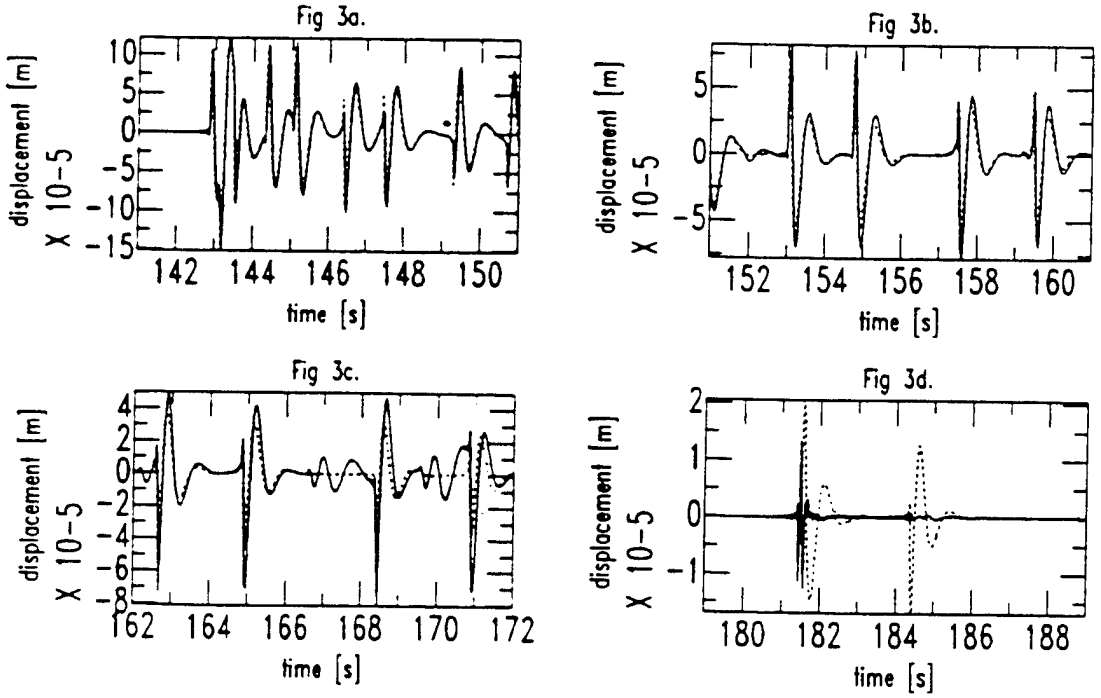

Figure 3. Comparison between seismograms computed using mode theory (solid lines) and ray theory (dashed lines). The epicentral distance is 500 km.

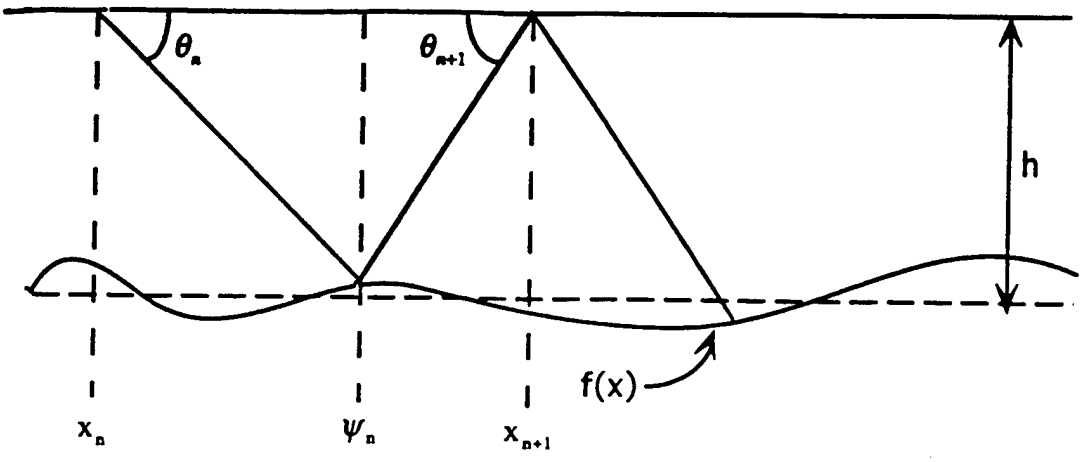

Figure 4. Geometry of layer over halfspace model with undulating discontinuity.

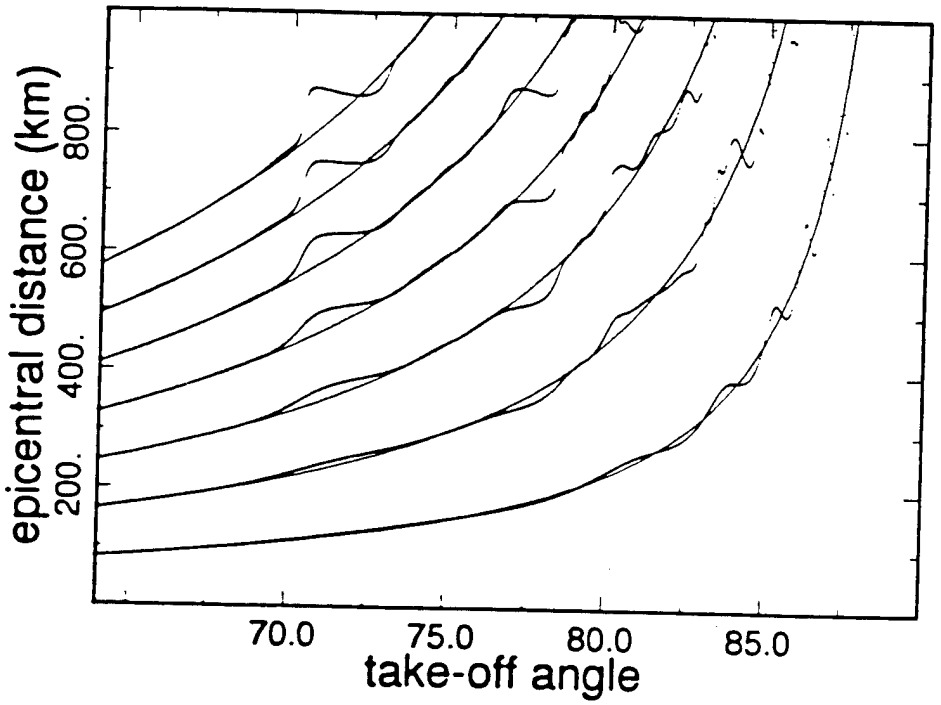

Figure 5. Epicentral distance as a function of take-off angle for *SmS* (bottom curve) through 7x *SmS* (top curve). Also plotted are the background values for a crust with a thickness of 20 km.

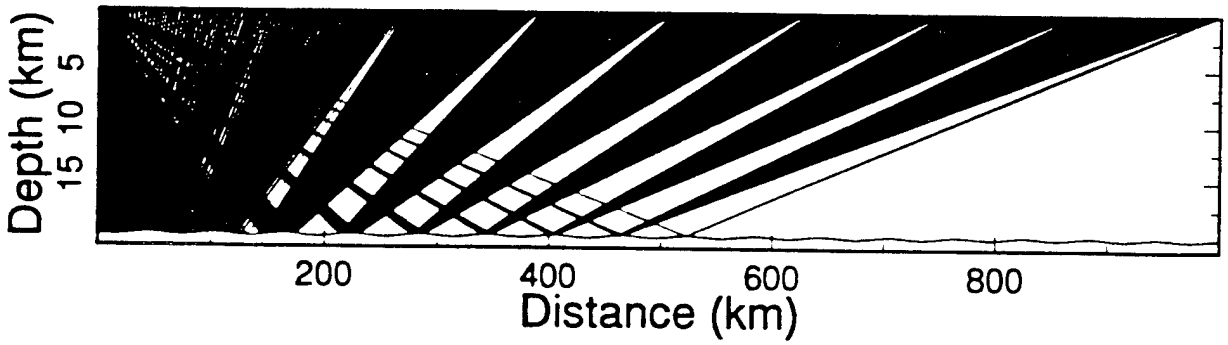

Figure 6. Ray paths for *SmS* from a surface source in a 20-km-thick crust, with sinusoidally undulating Moho of amplitude 0.1 km and period 60 km. Vertical exaggeration ×10.

Effects of Explosion Depth and Crustal Heterogeneity on *Lg* Waves

H. Keers, K. Vogfjörd, G. Nolet, F. A. Dahlen

Department of Geological and Geophysical Sciences, Princeton University, Princeton, NJ 08544

Contract number: F49620-94-1-0077

ABSTRACT

We use ray theory to model the propagation of *Lg* waves through 2D and 3D layered crustal models. The layers are homogeneous, and the discontinuities are undulating. The *Lg* wave train is modelled by multiple *S* reflections within the crustal layers. The ray tracing system is reduced from a set of linear differential equations to a set of maps. If the medium has three or more discontinuities the number of multiples increases exponentially. Using a binary tree-searching method we systematically keep track of all multiples.

The ray behavior is chaotic for large take-off angles, causing multipathing of the crustal multiples. However, in the presence of mid-crustal discontinuities the rms *Lg* amplitude is stable, because of the distribution of the energy over a large amount of rays. The simplest case, a one layer over a halfspace model, already contains all the characteristics of wave propagation through the media under consideration.

To examine the source-depth and velocity-structure effects on amplitudes and character of *Lg* we use wavenumber integration methods in 1-D structures. In particular, we study the ability of shallow explosions to generate S^* and *pS* rays. Although S^* is a nongeometrical phase it does follow a well defined raypath. In velocity structures, where the peak in the S^* radiation pattern is confined to the crust, signals from explosions within 1 km of the surface, that do not generate spall or significant tectonic release, are likely to be dominated by waves with a very narrow ray-parameter range, coming from the radiation peak of S^*. Observation of *Lg* waves dominated by such a narrow ray-parameter range may therefore identify the source as explosive, and shallow. Dislocation radiation patterns, or the spalls CLVD term are likely to generate significant *S* waves over a wider range of ray parameters and therefore not to be confused with S^*.

Effects of Explosion Depth and Crustal Heterogeneity on *Lg* Waves

OBJECTIVE

The objective of our research is to understand aspects of the excitation of *Lg* waves and their subsequent propagation through the crust, including 2D and 3D heterogeneous crustal models.

Modeling the *Lg* wave train is a difficult task, even though measurements of rms amplitude of *Lg* is stable. We attempt to explain this by modeling *Lg* as a superposition of supercritically reflected crustal multiples. In our models the crust is multilayered (2D or 3D) and the interfaces are undulating.

We also examine the effect S^* has on amplitudes and character of *Lg* to determine to what depths and in which types of velocity structures S^* is a significant contributor to *Lg*.

RESEARCH ACCOMPLISHED

Lg Wave Propagation Through 3D Heterogeneous Structures

To study the propagation of *Lg* waves through 2D and 3D heterogeneous media we use ray theory. Ray theory is not only very efficient, it also makes the characterization of *Lg* waves in terms of focusing/defocusing effects, multipathing and traveltimes due to the complicated structure relatively simple. Thus ray theory complements full waveform methods such as finite differences.

Lg waves possess a dual character (e.g. Hansen et al., 1990). On one hand the modeling of *Lg* waves has proved to be very difficult, on the other hand the *Lg* wavetrain has been useful to determine seismic moments because rms *Lg* is a stable quantity, that is relatively independent of regional structure. Using our modeling results we give an explanation for this seemingly contradictory character.

The models that we use are 2D and 3D layered crustal models. The layers are homogeneous, and the discontinuities are undulating. The *Lg* wave train is modelled by multiple *S* reflections within the crustal layers. In a flat layered medium the ray-theoretical seismograms are almost identical to the exact synthetics (Keers et al., 1995a). This serves as our justification for the use of ray theory in media with (slightly) undulating interfaces separated by homogeneous layers.

One of the main advantages of using homogeneous layers is that the ray tracing system can be reduced from a set of linear differential equations to a set of maps (Keers et al., 1994). This makes the ray tracing very efficient; it is not necessary to use a Runge-Kutta method and the search for the point where the ray intersects one of the undulating interfaces is reduced to a 1D root-solving problem (even in the three dimensional case). If the medium has three or more discontinuities the number of multiples increases exponentially. Using a binary tree-searching method we systematically keep track of all multiples.

The simplest case, a one layer over a halfspace model, already contains all the characteristics of wave propagation through the media under consideration. In general two regions (by regions we mean take-off angle intervals) are distinguished. One region, corresponding to smaller take-off angles, has regular ray-behavior, and another region, corresponding to the largest take-off angles, has chaotic ray-behavior. In the case of a sinusoidal Moho with a wavelength of 100 km and an amplitude of 1 km the take-off angle intervals are roughly 50°-65° and 65°-90° (the critical angle is close to 50°). The first region is characterized by a low degree of multipathing and a high degree of focusing. The second region is characterized by a large degree of multipathing and consequently a large degree of defocusing The defocusing is caused by the fact that a small change in take-off angle causes a large change in epicentral distance, except at the caustics. However, at the caustics the amplitude is still relatively small (Keers et al, 1995a). It should be noted that the amplitude perturbations due to the undulation are much larger than the traveltime perturbations. Table 1 gives an

indication of the degree of multipathing for the case of a flat Moho, a sinusoidal Moho and a more realistic model, that of the Moho below Germany.

In the case of a more realistic two-layered model with undulating interfaces, the ray behavior remains essentially the same: there exists a regular region corresponding to smaller take-off angles and a chaotic region corresponding to larger take-off angles. All discontinuities are sinusoidal. The surface has a wavelength of 60 km and amplitude of 0.5 km, the midcrustal discontinuity has a wavelength of 160 km and an amplitude of 0.8 km and the Moho has a wavelength of 100 km and an amplitude of 1.5 km. Figure 1a shows the amplitude distribution. This figure is essentially an 'envelope record-section'. It contains only amplitude information; no phase information. The strong focusing in the regular region that was present in the one-layered model is gone. This is due to the reflection and transmission of the multiples at the midcrustal interfaces, which partitions the energy over many multiples. The presence of the chaotic region makes it impossible to identify even the major multiples (SmS, $2SmS$ etc.) at larger epicentral distances. The large degree of multipathing of a certain multiple, like $2SmS$, causes these multiples to consist of many rays, each with a relatively small amplitude, coming in from totally different directions. Each of these multiples is smeared out over a larger time interval and the the maximum amplitude of the dominant rays is low compared to the flat layered case. This explains why the modeling of Lg waveforms has been largely unsuccesful: the waveform is very sensitive to initial conditions (take-off angle) and model parameters.

Figure 2a shows the effect of a 3D sinusoidal Moho. The wavelength is 100 km in both the x and y directions, and the amplitude is 1 km. The figure shows the energy distribution along the x axis. Also shown is the energy distribution for a 2D model with a sinusoidal Moho that has a wavelength of 100 km and amplitude of 1 km. The amount of side scattering can not be ignored, but depends strongly on the model (Keers et al, 1995b). Since this 3D example is for a one-layered model, the focusing of the different multiples plays a dominant role in this figure.

Figure 2b shows the total energy of the Lg wavetrain as a function of epicentral distance for the two models of figure 1. Also plotted is the energy of the waves assuming a $\Delta^{-5/6}$ (Nuttli, 1973) decay of the amplitude (Δ=distance). The undulating two-layered model shows much less focusing especially at larger epicentral distances. This is due to the midcrustal interface. There is still focusing of certain rays, but the reflection and transmission from the midcrustal interface makes these rays much less dominant than in the one-layered model. This explains the stability of rms Lg as observed for many regional events (e.g. Hansen et al., 1990). For models with more layers we can expect the focusing effects to become even less dominant.

Effects of Source Depth and Velocity Structure on the Character of Lg

Discrimination between shallow sources is a difficult task and methods, such as Pg/Lg amplitude ratios and Lg spectral ratios as well as regional m_b:M_S, seem to be region dependent and only work for discrimination between shallow explosions and earthquakes deeper than 5 km, and even then there are problems with explosion depths of <1 km. Generation of S waves from explosion sources has generally been attributed to nonisotropic source radiation, spall, tectonic release, or Rg-S scattering in the source region, while S^*, the wave generated by interaction between the curved P wave-front and the surface, has usually been discounted for all but the shallowest sources, because of its strong dependence on source depth. However, due to the S^* radiation pattern, in certain structures the amplitude may be significant down to depths of $\sim$1 km, possibly making S^* an added tool to discriminate between shallow sources.

To examine the source-depth and velocity-structure effects on amplitudes and character of Lg we use wavenumber integration methods in 1-D structures. The shortcomings of the simplified structure are overcome by the benefits of a full-wave synthesis, revealing all waves generated by the source and its interaction with discontinuities in the structure; of main interest, of course, is the interaction with the Earth's surface. The characteristics observed in the synthetics are then explained in terms of the radiation pattern of S^*.

A high frequency approximation to the amplitude and phase of the S^* wave was developed by Daley and Hron (1983). In this approximation S^* appears as a spherical wave-front with SV-particle motion, radiated from a point on the surface above the source. Its amplitude is modulated as a function of angle ϕ (measured from the vertical), but is independent of azimuth. The wave exists for $\phi_d = \sin^{-1}(\beta/\alpha) \leq \phi \leq \pi/2$, but the approximation is valid for $\phi_d < \phi < \pi/2$, or $1/\alpha < p < 1/\beta$, where α and β are the mediums P and S

velocities and $p = \sin\phi/\beta$, is the ray parameter. A plot of the radiation function for a frequency of 2 Hz and $\alpha = 4.2$ km/s is shown in Figure 3 (top right). The source depths represented are: 0.1, 0.5, 1.0 and 2.0 km. The amplitude is a maximum at ϕ_d, but decreases to zero at $\phi = 45°$, where the phase also flips by 90°. The amplitude increases again to a smaller maximum, before becoming zero again at 90°. The amplitude decays exponentially with source depht, so for depths greater than 0.5 km, amplitudes are very small at angles above 45°. However, between ϕ_d and 45° the amplitude can be larger than in the original P and the reflected pS wave. To demonstrate, the pS radiation pattern, which exists for reflection angles $\phi < \phi_d$, is also included on the plot.

If the narrow radiation peak of S^* gets trapped in the crust, it may dominate Lg. To demonstrate we calculated synthetics in three different velocity structures, md1, where the peak is radiated into the mantle, md2, where the peak is confined to SmS multiples for source depths down to 1.25 km and, md3, where the peak is confined to turning waves in the crust for source depths down to 1 km. The models have a common Q structure and share a velocity structure below 3 km depth (see Figure 4, lower panel). It is the ratio $\alpha_{source}/\beta_{mantle}$ that determines how much of S^* is trapped in the crust. If $\alpha_{source} < \beta_{mantle}$, all of S^* and some pS are contained in Lg, but when α_{source} increases to $\geq \beta_{mantle}$ the radiation peak starts to go into the mantle. When the critical angle for Moho reflection exceedes $\sim 42°$, no significant S^* can be found in Lg, except for depths $\leq$0.5 km. The angular range of Moho reflections in the three models is indicated on Figure 3 (top right). There it is clear that in md1, most of the S^* radiation peak goes into the mantle and therefore Lg, from a pure explosion source, is expected to decay quickly with source depth. However in md2, all of the radiation peak ends up in Moho reflections, for source depths down to 1.25 km. For this depth range Lg is expected to be of significant amplitude and to be dominated by Moho reflections. In md3, the peak is confined to turning waves in the crust, for source depths down to 1 km. In this depth range Lg is also expected to be significant and dominated by turning waves. These effects are clearly seen in the synthetics: In Figure 4, synthetics are shown at a distance of 500 km for source-depths ranging from 0.1 to 2 km in model md2. Clearly the Lg wave is dominated by the Moho multiples, $2SmS$, $3SmS$ and $4SmS$, and Lg amplitude is significant for source depths down to $\sim$1 km. Record sections for an explosion source at 0.5 km depth in the three models are shown in Figure 5, where the expected features are also seen. The md1 record section has smaller amplitude Lg waves than the other models, evenly divided between Moho reflections and turning waves. The frequency content of the Lg wave is also significantly lower than that of the crustal P wave-train. The md2 record section has much larger amplitudes, Lg is dominated by Moho multiples, and there is no significant loss of higher frequencies in Lg. The md3 record section has large amplitude Lg waves of high frequency content, and maximum amplitudes coincide with the arrivals of the turning waves and Moho reflections; the Moho reflections come from pS and the turning waves come from S^*.

Analysis of Array Data

The theoretical results need to be tested against observed data from local and regional events. We have so far selected two regions based on the availability of short-period array data. The regions are: Central Europe, where we make use of the GERESS array, and the Sierra Nevada, where three, 3-component arrays were temporarily operated in 1993. The arrays enable detection of small coherent arrivals and decomposition of the Lg wave train into distinct arrivals with differing phase velocities. The events recorded at GERESS consist of earthquakes and explosions, while most of the events recorded on the Sierra Nevada arrays are earthquakes, but also include the NPE explosion at the Nevada Test Site in September 1993.

CONCLUSIONS AND RECOMMENDATIONS

In 2D and 3D heterogeneous media Lg wave propagation is strongly affected by curved interfaces. The ray behavior is chaotic for large take-off angles, causing multipathing of the crustal multiples. This makes modeling of Lg waves a tidy task. However, in the presence of mid-crustal discontinuities rms Lg is stable, because of the distribution of the energy over a large amount of rays. It should be noted that the undulations used are small (of the order of 1 km). The amplitude behavior will change if the undulations of the Moho become large. Further research is needed to establish this effect. Incorporation of P-S and S-P conversions using our ray-tracing algorithm should make it possible to model Lg wave propagation more realistically.

More detailed Moho maps for regions of interest are also necessary for reliable modeling of *Lg* in 3D structures. This goal can be achieved by wave-form inversion, using regional seismograms (Das and Nolet, 1995).

In velocity structures, where the peak in the S^* radiation pattern is confined to the crust, signals from explosions within 1 km of the surface, that do not generate spall or significant tectonic release, are likely to be dominated by waves with a very narrow ray-parameter range, coming from the radiation peak of S^*. Observation of *Lg* waves dominated by such a narrow ray-parameter range may therefore identify the source as explosive, and shallow. Dislocation radiation patterns, or the spalls CLVD term are likely to generate significant *S* waves over a wider range of ray parameters and therefore not to be confused with S^*. A comparison between data from mining explosions and earthquakes, located in approximately the same area, may serve as a test case for this. GERESS data for events in the Vogtland region in the Csech Republic may be possible candidates.

The completed record section profiles will serve as the data base needed to test the validity of the theoretical calculations and predictions.

REFERENCES

Daley, P. F. and F. Hron (1983). High-frequency approximation to the nongeometrical S^* arrival, *Bull. Seism. Soc. Am.*, 73, 109-123.

Das, T. and G. Nolet (1995). Crustal thickness estimation using high frequency Rayleigh waves, *Geophys. Res. Lett.*, 22, No. 5, 539-542.

Hansen, R. A., F. Ringdal and P. G. Richards (1990). The Stability of RMS *Lg* Measurements and Their Potential for Accurate Estimation of the Yields of Soviet Underground Nuclear Explosions, *Bull. Seism. Soc. Am.*, 80, 2106-2126.

Keers, H., G. Nolet and F. A. Dahlen, 1995a. Ray Theoretical Analysis of *Lg*, (submitted to *Bull. Seism. Soc. Am.*).

Keers, H., G. Nolet and F. A. Dahlen, 1995b. Chaos and *Lg* Waves, EOS, volume 76, no 17, 205.

Keers, H., K. Vogfjörd, G. Nolet and R. Phinney, 1994. *Lg* Synthesis in Media With Undulating Surfaces by Ray Summation, EOS, volume 75, no 44, 420.

Nuttli, O. W. (1973). Seismic wave attenuation and magnitude relations for Eastern North America, *J. Geophys. Res.*, 78, 876-885.

Vogfjörd, K. S. (1995). Effects of explosion depth and Earth structure on excitation of *Lg*: S^* revisited, (submitted to *Bull. Seism. Soc. Am.*).

Table 1 | Number of supercritically reflected rays for different Moho models

epicentral distance (km)	flat Moho	Sinusoidal Moho	Moho below Germany
200	4	4	17
300	6	6	26
400	8	10	53
500	10	14	140
600	12	22	216
700	15	31	218
800	17	56	270

Table 2	layer #	thickness (km)	S-velocity (km/s)	density (g/cm3)
	1	15	3.5	2.7
	2	15	3.9	3.1
	3	∞	4.6	3.3

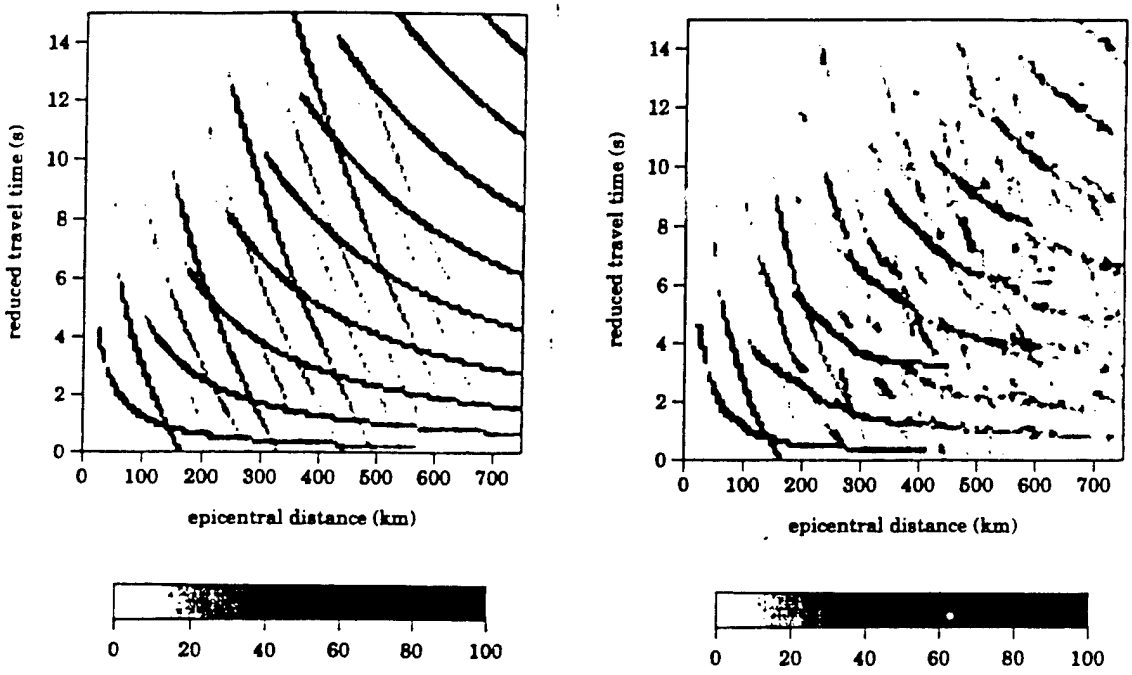

Figure 1. Amplitude distribution for two-layered crustal model with flat interfaces (left) and undulating interfaces (right; see text for the characteristics of the undulations). The amplitudes are scaled with respect to the maximum value (100).

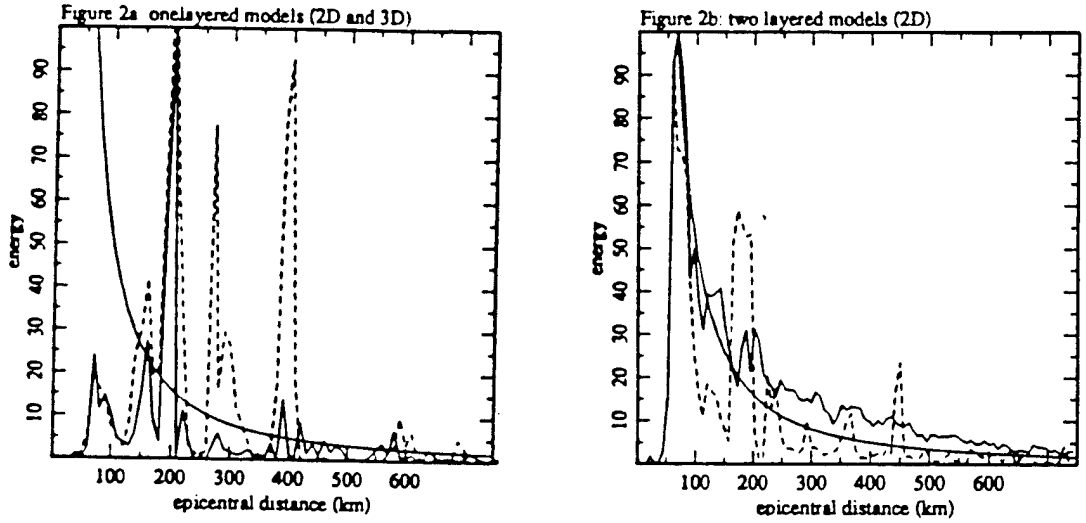

Figure 2a. Energy distribution for a one-layered crustal model with undulating Moho (see text) for 2D (solid) and 3D (dashed) model. The decay of energy according to Nuttli (1973) is also shown (smooth curve).

Figure 2b. Energy distribution for same models as in figure 1: flat model (solid) and model with undulating discontinuities (dashed). The smooth curve is the decay of energy according to Nuttli (1973).

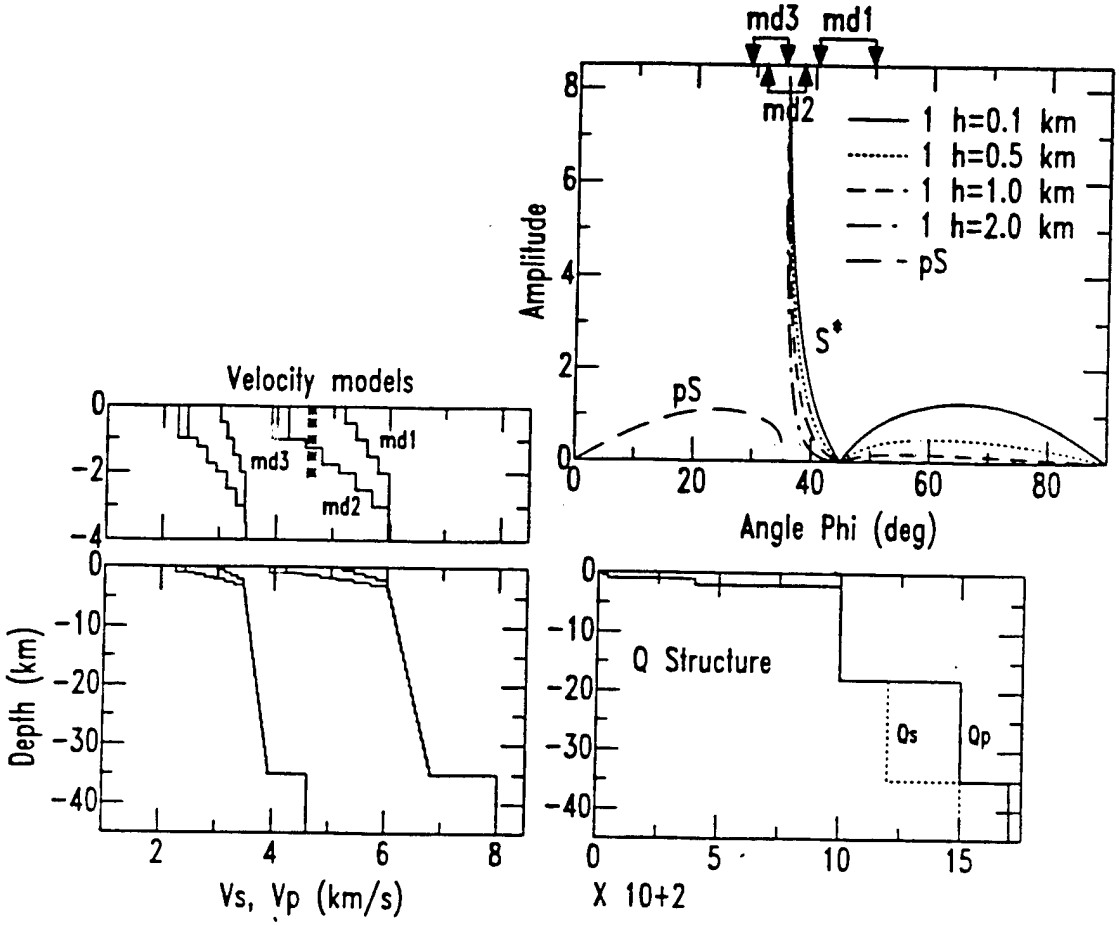

Figure 3. (upper right) S^* radiation pattern at 2 Hz, for various source depths in a medium with $\alpha = 4.2$ km/s. Velocity models (left) and Q structure (lower right) used in the synthetic calculations. Stars, representing some of the source depths used, are positioned at the sub-Moho S velocity, β_{mantle}.

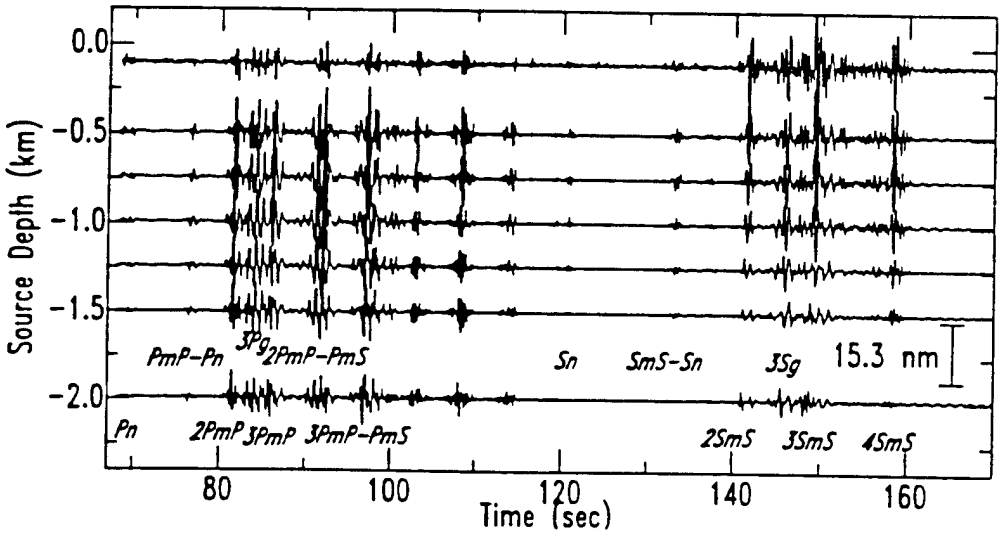

Figure 4. Vertical component synthetic displacement at 500 km distance from an explosion source at various source depths in model md2. The synthetics have a Nyquist frequency of 4 Hz and are convolved with a NORESS-type short-period instrument.

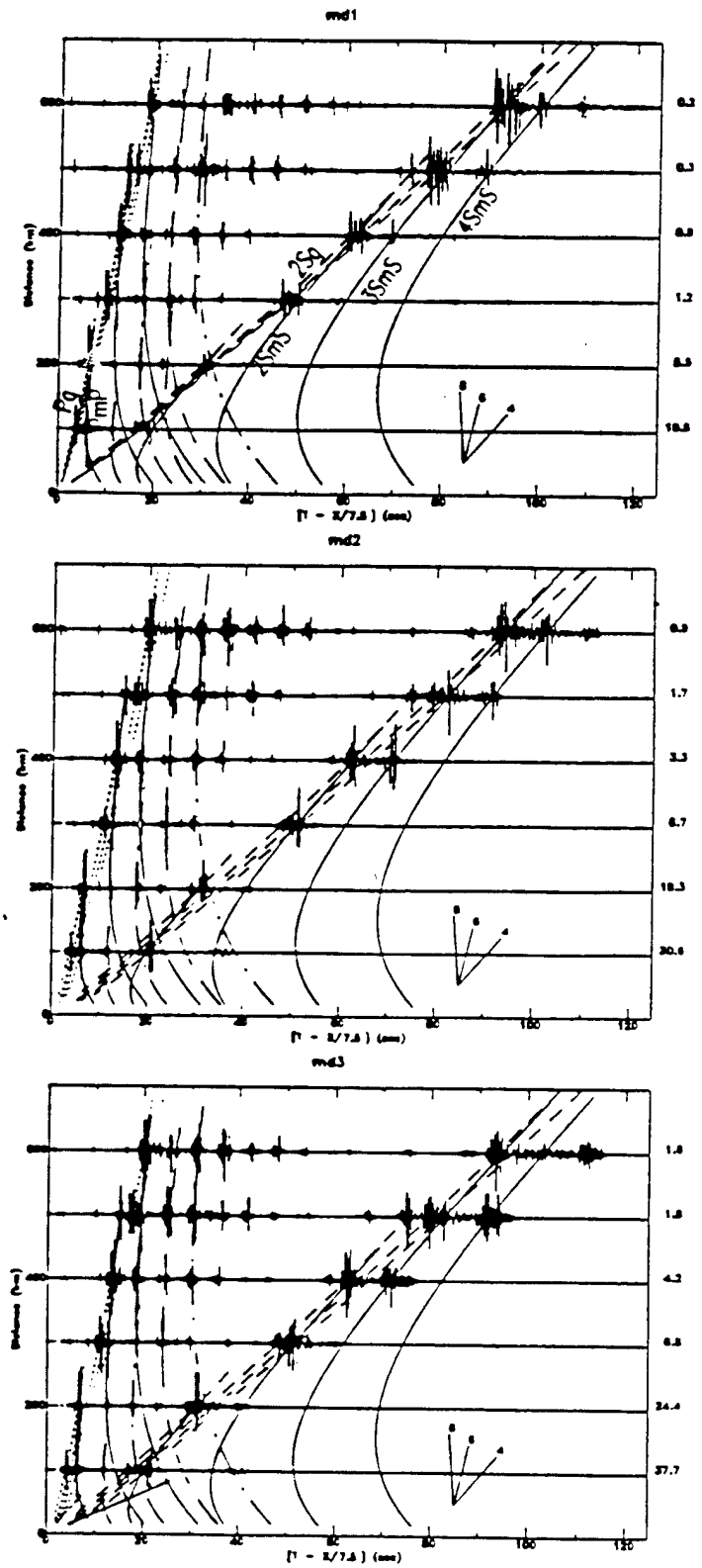

Figure 5. Vertical component synthetic record sections for an explosion depth of 0.5 km in the three models, md1, md2 and md3, with travel-time curves for the major phases superimposed. Amplitudes are normalized to their maxima, shown at the right of each trace. Slopes on the travel-time curves can be read from the velocity template in the lower right corner.

HIGH FREQUENCY PROPAGATION OF CRUSTAL WAVES

H. Keers, K. Vogfjörd, G. Nolet, F. A. Dahlen
Department of Geosciences, Princeton University, Princeton NJ 08544
Contract No. F49620-94-1-0077
Sponsored by AFOSR

ABSTRACT

This report discusses both theoretical and observational aspects of asymptotic crustal wave propagation.

Crustal models (both 2D and 3D) are conveniently expressed using undulating interfaces. This makes it necessary to develop special ray tracing algorithms (both for the kinematic and dynamic ray tracing). These algorithms and the chaotic properties of rays traveling through these models are discussed briefly.

One consequence of the chaotic ray behavior is the large number of caustics that are generated. This makes it necessary to use Maslov theory to compute synthetics, rather than geometrical ray theory. It is shown in this report how to compute the correct Maslov phase and amplitude using the method of stationary phase.

One of the major obstacles in computing Maslov synthetics has been the presence of spurious arrivals caused by pseudo-caustics. Using the method of stationary phase these pseudo-caustics are shown to disappear if one uses 2D Maslov integrals. An algorithm is presented that efficiently computes 2D Maslov integrals. Previously Maslov synthetics were plagued by the effect of the endpoints of the integration. This endpoint effect is removed by a simple change of variables.

The Maslov synthetics can be used to justify the use of ray density plots as energy plots. The ray density plots are used to study array data from the NPE at the Nevada test site. Lg waves, propagating in the direction of the southern Sierra Nevada range, disappear in the epicentral distance r ıge of 250 km - 350 km. It is shown how the theoretical modeling of Lg can be used to put constraints on the crustal structure of sourthern California.

Keywords: crustal waves, chaotic rays, Maslov synthetics, energy plots, array data

OBJECTIVES

The first goal of this project is to develop reliable and efficient methods to compute synthetic seismograms through 2D and 3D heterogeneous crustal models, using asymptotic methods. The second goal of this project is to apply these methods to study crustal wave propagation (with special emphasis on Lg) using array data. Both of these aspects are discussed in this report.

RESEARCH ACCOMPLISHED

Kinematic Ray Tracing Through 3D Multilayered Media

We briefly describe raytracing in 3D layered media with undulating interfaces separated by homogeneous layers. Two aspects are important: first one needs to trace rays from one interface to the next interface. Secondly all multiples generated need to be traced. Here, for the sake of conciseness, we only consider the first aspect of the algorithm; for more details see Keers et al. (1996b).

The interfaces are described by the equation $z = h_p + f_p(x, y)$ and, as before, the pth layer is right below the pth interface. We choose the coordinate system as shown in figure 1.

Consider a ray impinging upon the pth interface from above. The unit vector pointing in the direction of the ray is $\mathbf{i_n} = (\cos\alpha_n, \cos\beta_n, \cos\gamma_n)$ (see figure 1). This vector is assumed to be known. The unit normal to the pth interface at $(x_n, y_n, h_p + f_p(x_n, y_n))$ is denoted by $\mathbf{n} = (n_1, n_2, n_3)$. From figure 2 it can be seen that $\mathbf{r}_n = 2(\mathbf{i}_n \cdot \mathbf{n})\mathbf{n} - \mathbf{i}_n$, where $\mathbf{r}_n$ is the unit vector pointing in the direction of the reflected ray. The derivation of $\mathbf{t}_n$ is a bit more involved. From figure 2 we see that

$$\mathbf{t}_n - (\mathbf{t}_n \cdot \mathbf{n})\mathbf{n} = c(\mathbf{i}_n - (\mathbf{i}_n \cdot \mathbf{n})\mathbf{n}), \tag{1}$$

for some $c < 0$. We compute c by taking the inner product of (1) with $\mathbf{i}_n$ and $\mathbf{t}_n$ respectively. We find

$$\mathbf{t}_n = (\mathbf{t}_n \cdot \mathbf{n})\mathbf{n} + \mathbf{t}_n - (\mathbf{t}_n \cdot \mathbf{n})\mathbf{n} = -\left(\frac{\alpha_{p+1}}{\alpha_p}\right)\mathbf{i}_n + \left(\left(\frac{\alpha_{p+1}}{\alpha_p}\right)(\mathbf{i}_n \cdot \mathbf{n}) - \cos\psi\right)\mathbf{n}. \tag{2}$$

Here ψ is found with Snell's law. These results enable us to derive the raytracing equations. If a ray goes up then direction vector is denoted by $\mathbf{u}_n^p$. If the ray goes down then the direction vector is $\mathbf{d}_n^p$. It can be shown that

$$h_p + f_p(x_n^p, y_n^p) + \left(\frac{u_{n,x}^p}{u_{n,x}^p}\right)(x_{n+1}^{p-1} - x_n^p) = h_{p-1} + f_{p-1}(x_{n+1}^{p-1}, y_n^p + \left(\frac{u_{n,y}^p}{u_{n,x}^p}\right)(x_{n+1}^{p-1} - x_n^p)) \tag{3}$$

which is an implicit equation for x_{n+1}^{p-1},and

$$y_n^p + \left(\frac{u_{n,y}^p}{u_{n,x}^p}\right)(x_{n+1}^{p-1} - x_n^p) = y_{n+1}^{p-1}. \tag{4}$$

The reflection vector $\mathbf{d}_{n+1}^{p-1}$ and the transmission vector $\mathbf{u}_{n+1}^{p-1}$ are found using the formulas given above and the correct choice of orientation of $\mathbf{n}$. In vector notation:

$$\mathbf{i}_{n+1}^{p-1} = -\mathbf{u}_n^p \tag{5}$$

$$\mathbf{d}_{n+1}^{p-1} = 2(\mathbf{u}_n^p \cdot \mathbf{n})\mathbf{n} + \mathbf{u}_n^p \tag{6}$$

$$\mathbf{u}_{n+1}^{p-1} = \left(\frac{\alpha_{p-2}}{\alpha_{p-1}}\right)\mathbf{u}_n^p + \left(\left(\frac{\alpha_{p-2}}{\alpha_{p-1}}\right)(\mathbf{u}_n^p \cdot \mathbf{n}) - [1 - \left(\frac{\alpha_{p-2}}{\alpha_{p-1}}\right)^2 (1 - (\mathbf{u}_n^p \cdot \mathbf{n})^2)]^{1/2}\right)\mathbf{n}. \tag{7}$$

Similar formulas can be derived for the downgoing ray (Keers et al, 1996b).

Dynamic Ray Tracing

We now proceed to derive the partial derivatives of the kinematic ray equations. It is clear that in 3D media the parameters that give the ray positions are: x_n, y_n and $\mathbf{d}_n$ (the superscripts p and $p-1$ are deleted from now on). All the other parameters are found from these. In particular we shall be interested in the dependence of these parameters on the initial take-off angle θ_0. These are necessary in establishing the degree of chaoticity using Lyapunov exponents and the computation of synthetics with Maslov integrals (see the next two sections). In 3D media $\mathbf{d}_n$ has three components and for the computation of the Maslov amplitude we also need the dependence of x_n, y_n and $\mathbf{d}_n$ on the initial azimuth δ_0. The differentation can be computed by perturbing the ray equations with the appropriate parameter (e.g. δx_n) and then derive expressions of the form

$$\frac{\delta x_n}{\delta x_{n+1}} \tag{8}$$

Taking the limit gives the required partial derivative. For brevity we only give some of the partial derivatives. Note that, whenever possible, use should be made of the vector notation. As in the case of the kinematic ray tracing this considerably reduces the algebraic effort. One finds

$$\frac{\partial x_{n+1}}{\partial x_n} = \left(r_1 - \frac{\partial f_{p-1}}{\partial y_{n+1}}\frac{\partial y_{n+1}}{\partial x_n}\right) / \left(r_1 - \frac{\partial f_p}{\partial x_n} + \frac{\partial f_{p-1}}{\partial y_{n+1}}\frac{\partial y_{n+1}}{\partial x_n}\right), \tag{9}$$

etc. where

$$r_1 = \frac{r_{n,x}}{r_{n,x}}, \tag{10}$$

$$r_2 = \frac{r_{n,y}}{r_{n,x}}. \tag{11}$$

$$\frac{\partial d_{n+1}}{\partial x_n} = 2[(\mathbf{u}_n \cdot \partial_{x_n}\mathbf{n})\mathbf{n} + (\mathbf{u}_n \cdot \mathbf{n})\partial_{x_n}\mathbf{n}], \tag{12}$$

etc. Similar partial derivatives are derived for the upgoing ray.

Chaotic Ray Behavior and Lyapunov Exponents

We showed previously (Keers et al., 1996a) that a small change in the take off angle gives rise to a large change in the epicentral distance. This chaotic behavior can be quantified using the concept of Lyapunov exponents. The idea is to measure the separation d between two points in phase space that are initially together. Note that two points in phase space are close together only if they are

at almost the same position in coordinate space and if, in addition to that, the slownesses of the rays emanating from these points are almost the same as well.

If the ray tracing system is chaotic then, by definition, the separation rate of the two points in phase space is exponential. In other words there is a constant $l > 0$ such that

$$e^{nl} = d(n), \tag{13}$$

In order to illustrate this we use the 2D version for a one layered model of the kinematic and dynamic ray equations derived above. After scaling x with the thickness of the crust one can define $M(\theta_n, x_n) = (\theta_{n+1}, x_{n+1})$ and

$$D(\theta_n, x_n) = \begin{pmatrix} \frac{\partial \theta_{n+1}}{\partial \theta_n} & \frac{\partial \theta_{n+1}}{\partial x_n} \\ \frac{\partial x_{n+1}}{\partial \theta_n} & \frac{\partial x_{n+1}}{\partial x_n} \end{pmatrix} \tag{14}$$

Let $y_n = (\theta_n, x_n)$ and $\delta y_n = (\delta\theta_n, \delta x_n)$.If $\delta\theta_n$ and δx_0 are small then y_0 and $y_0 + \delta y_0$ are close together. After one iteration we have $y_1 = M(y_0)$. Since $\mid \delta y_0 \mid$ is very small $M(y_0 + \delta y_0)$ may be approximated by $M(y_0) + D(y_0)\delta y_0 = y_1 + D(y_0)\delta y_0$. Therefore $\delta y_1 \approx D(y_0)\delta y_0$. More generally $\delta y_n = D(y_{n-1})\delta y_{n-1} = D^n(y_0)\delta y_0$, where $D^n(y_0) = D(y_{n-1})D(y_{n-2}) \cdot D(y_0)$. The distance between y_0 and $y_0 + \delta y_0$ after n iterations can therefore be approximated by $\mid \delta y_n \mid = \mid D^n(y_0)\delta y_0 \mid$. The rate of divergence l between y_0 and y_0 and $y_0 + \delta y_0$ is therefore given by

$$e^{nl} = \frac{\mid \delta y_n \mid}{\mid \delta y_0 \mid} \tag{15}$$

In principle l depends on y_0, δy_0 and n: $l = l(y_0, \delta y_0, n)$. However l can be shown to be independent of the initial conditions, and to converge to a constant as $n \to \infty$. Therefore it is useful to define the Lyapunov exponent l_L:

$$l_L(\theta_0, x_0) = \lim_{n \to \infty} \frac{1}{n} \frac{D^n(y_0)\delta y_0}{\mid \delta y_0 \mid} \tag{16}$$

When explicitly computing the Lyapunov exponents we use the method of Benettin et al. (1980). Choose $(\delta\theta_0, \delta x_0)$ arbitrary and rescale $(\delta\theta_n, \delta x_n)$ every p iterations by dividing by its magnitude. In this way numerical overflow is avoided. If we do this q times and denote the resulting scaling factors by $s_i (i = 1, \cdots, q)$ then

$$l_L \approx \frac{1}{qp} \sum_{i=1}^{l} \ln s_i \,. \tag{17}$$

In practice we choose $p = 10$ and $q = 100$. Figure 3b shows the results of the computation of 9 Lyapunov exponents. The corresponding solutions of the rays in phase space are shown in figure 3b. The Lyapunov exponents of all the rays converge to a certain value. In fact, since they converge relatively rapidly, we could have taken $q = 50$. The most chaotic ray in figure 3b with an initial take-off angle of 70°, has a Lyapunov exponent of 0.8. This means that rays that are initially 100 m apart, after ten reflections from the Moho are almost 300 km apart; this strongly chaotic behavior results in a large degree of multipathing and many caustics. When computing synthetics it therefore is necessary to use an algorithm that easily can handle these phenomena. The major candidate for this is Maslov theory.

Maslov Theory and Pseudo-caustics

An acoustic wavefield u excited by a point source at x_0 at time 0 satisfies

$$\nabla^2 u(\mathrm{x},t) - \frac{1}{c^2(\mathrm{x})}\frac{\partial^2}{\partial t^2}u(\mathrm{x},t) = \delta(\mathrm{x}-\mathrm{x}_0)\delta(t) \tag{18}$$

If we define the Fourier transform as

$$\hat{f}(\omega) = \int_{-\infty}^{\infty} f(t)e^{-i\omega t}dt \tag{19}$$

then the wave equation can be transformed to the frequency domain and we have

$$\nabla^2 \hat{u}(\mathrm{x},\omega) + k^2(\mathrm{x})\hat{u}(\mathrm{x},\omega) = \delta(\mathrm{x}-\mathrm{x}_0) \tag{20}$$

Here $k = \omega/c$. In Maslov theory one looks for solutions of the form

$$\hat{u}(\mathrm{x},\omega) = \int \mathcal{A}(\mathrm{x},q)e^{i\omega\mathcal{T}(\mathrm{x},q)}dq \tag{21}$$

and

$$\hat{u}(\mathrm{x},\omega) = \int\int \mathcal{A}(\mathrm{x},q_1,q_2)e^{i\omega\mathcal{T}(\mathrm{x},q_1,q_2)}dq_1 dq_2 \tag{22}$$

Whenever both asymptotic ray theory (ART) and one of the Maslov integrals are valid then the ART solution can be obtained from the Maslov integrals by applying the method of stationary phase. One advantage of this is, that the Maslov amplitude can easily be found. Application of the method of stationary phase to the 1D Maslov integral gives the expression for $\mathcal{A}$. If we take q to be the initial take-off angle ϕ_0, then the wavefield becomes

$$\hat{u}(\mathrm{x},\omega) = \oint \mathcal{A}e^{i\omega\mathcal{T}}d\phi_0 \tag{23}$$

This has the advantage that the integration is over a closed circle. The usual boundary points therefore don't exist, and there are no spurious arrivals in the integral. Also the application of a taper at the boundaries becomes superfluous. The stationary phase method gives $\mathcal{A}$ again. Also in this case the we may take $(q_1,q_2) = (\phi_0,\theta_0)$, in which case the integral reduces to

$$\hat{u}(\mathrm{x},\omega) = \oint \mathcal{A}(\mathrm{x},\phi_0,\theta_0)e^{i\omega\mathcal{T}(\mathrm{x},\phi_0,\theta_0)}d\phi_0 d\theta_0 \tag{24}$$

It is worthwile to have a closer look at the singularities of the asymptotic wavefield expressions. Classical ray theory breaks down at points where $J = 0$ (J is the Jacobian from coordinate space to ray coordinates). Similarly the Maslov integrands are singular at points where $\mathcal{J} = 0$ (here $\mathcal{J}$ is the Jacobian from mixed phase space to ray coordinates). These points form pseudo-caustics. In the case of a 1D integral these points also correspond to stationary points. In the 2D integral the pseudo-caustics are given by

$$|\mathcal{J}| = 0 \tag{25}$$

However, stationary points are given by,

$$\frac{\partial p_1}{\partial q_1}(x-X)+\frac{\partial p_2}{\partial q_1}(y-Y)=0, \tag{26}$$

$$\frac{\partial p_1}{\partial q_2}(x-X)+\frac{\partial p_2}{\partial q_2}(y-Y)=0. \tag{27}$$

A singul: rity in the Maslov integral then would only be prominent whenever we have simultaneously a pseudo-caustic and a stationary point. Therefore pseudo-caustics are less troublesome in 2D integral expressions than in 1D integral expressions.

In the time domain we get the following expression for the Maslov wavefield

$$u(\mathrm{x},t)=\frac{1}{4\pi}\mathrm{Re}[\Delta(t)*\sum_{t=\mathcal{T}}\mathcal{A}\left(\frac{\partial\mathcal{T}}{\partial q}\right)^{-1}] \tag{28}$$

where $\Delta(t)=\delta(t)-i/\pi t$ is the analytic delta function. In the 1D case the integration is done similarly to the WKBJ evaluation of wavefields in 1D media following Chapman et al. (1988). In the 2D case we either are integrating over a plane or a sphere, as discussed previously. This requires a slight adaptation of the integration algorithm (subroutine THETAC (Chapman et al., 1988). The integration domain is triangulated (Delaunay triangulation for example) and a suitable taper is chosen in the case that the integration domain is plane. The Delaunay triangulation has the useful property that the 3 gridpoints closest to each point in a triangle form the triangle. The best linear approximation to a function at a point in the triangle that uses the gridpoints, is therefore given by the average of the values of that function on the three vertices of the triangle.

Ray Density Plots and Lg Propagation in California

The Maslov method can also be used to justify the use of ray density plots as energy plots. Energy plots are useful for studying the crustal wavetrain as a whole. Figure 4 shows vertical component data from the Non Proliferation Experiment (NPE) at the Nevada Test Site. All data are highpassed at 2 s. Traveltime curves of PmP and SmS are shown as well as traveltime curves of other dominant crustal multiples. The source and station locations are shown in figure 5. We concentrate in this report on Lg. Using a three layered crustal model ray density plots are obtained for different models. In the case the model is flat the different multiples can be readily identified (figure 6a). However from the data it can be seen that Lg, while still strong at 270 km, quickly reduces in amplitude and is almost invisible in several records at distances larger than 300 km. More realistic models include crustal thickening under the Sierra Nevada and bumps in the midcrustal interfaces. The resulting ray density plot for a 10 km amplitude and 150 km wavelength bump is shown in figure 6b. If, in addition to these undulations, variations in the midcrustal interfaces are added (figure 6c) then Lg disappears at the required epicentral distance. Using the ray density plots it is possible to constrain the heterogeneity of the Moho between the NTS and the receivers. It was found that the bump in the Moho has its maximum just slightly to the east of the center of the Sierra Nevada. This result is rather independent of the strength of the heterogeneities in the midcrust. Figure 6d shows the ray density plots for a model like that in figure 6c, but with additional random undulations of the

midcrustal interface with an amplitude of 2 km and and a dominant wavelength of 100 km. The random structure has the effect to even out some prominent arrivals still present in figure 6c. Since the data do not show such arrivals, we prefer the last model.

CONCLUSIONS AND RECOMMENDATIONS

We show in this report how to compute ray paths through 2D and 3D layered crustal structures. These crustal models generate chaotic rays, the effect of which is to create many caustics and a high degree of multipathing. Using Maslov theory synthetics can be computed; the effect of pseudo-caustics was shown to disappear if 2D Maslov integrals are used. Maslov amplitudes are computed using dynamic ray tracing and the method of stationary phase.

The theory was applied to study Lg propagation in southern California. Array data from the NPE at the Nevada Test Site showed that Lg disappears at epicentral distances between 250 km and 350 km. By using ray density plots it was shown what crustal structure is needed in order to show this behavior.

The algorithm presented here concerns acoustic wave propagation. In order to study crustal waveforms in general, and not only Lg, it is necessary to extend the algorithm to include P-S and S-P conversion. This would also make it possible to study the change of P/Lg amplitude ratios. The use of ray density plots as energy plots should be justified using synthetics. An excellent method is provided by the Maslov algorithm presented in this paper. This algorithm also makes it possible to study effects of 3D heterogeneity. However this requires the existence of high quality array data.

REFERENCES

Benettin, G., Galagni, L., Giorgilli, A. and Strelcyn, J.-M., 1980. Lyapunov characteristic exponents for smooth dynamical systems and for Hamiltonian systems: a method for computing all of them. Part 2: numerical application, *Meccanica*, **15**, 21.

Chapman, C. H., Jen-Yi, C. and Lyness, D. G., 1988. The WKBJ Seismogram Algorithm, in *Seismological Algorithms*, Doornbos G. (ed.), *Academic Press*, 47-74.

Keers, H., Nolet G., and Dahlen F. A., 1996a. Ray Theoretical Analysis of Lg, *Bull. Seism. Soc. Am.*, **86**, 726-736.

Keers, H., Dahlen F. A., and Nolet G., 1996b. Chaotic Ray Behavior in Seismology, *Geoph. Journal. Int.*, submitted.

Keers, H., and Chapman C. H., 1996. Maslov Theory and Pseudo-caustics, in preparation.

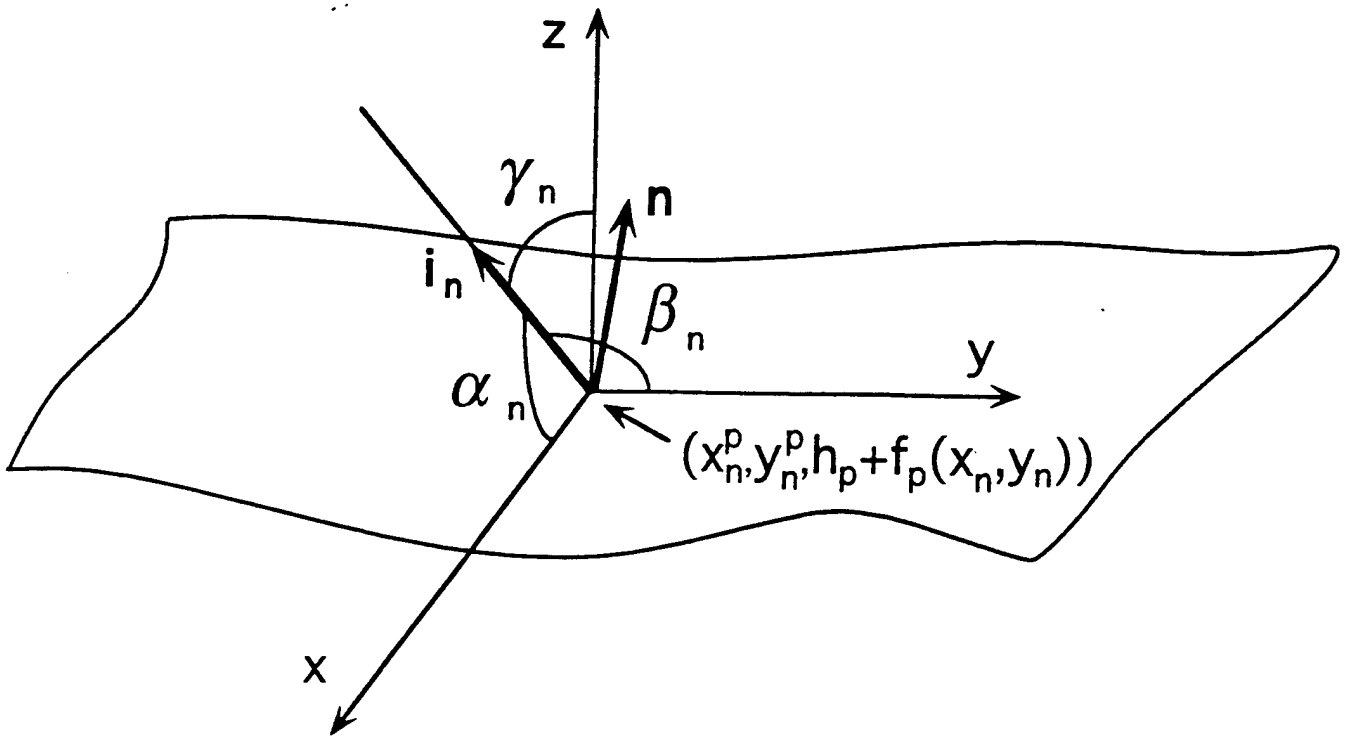

Figure 1. Definitions of ray tracing parameters used in the derivation of the kinematic ray equations.

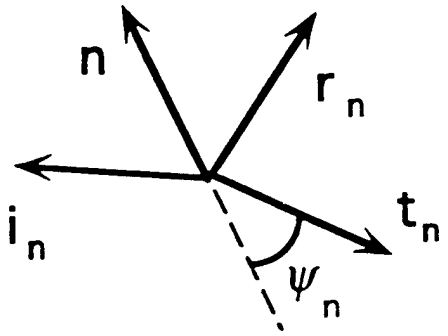

Figure 2. Definitions of the unit vectors and angle used in the kinematic ray equations.

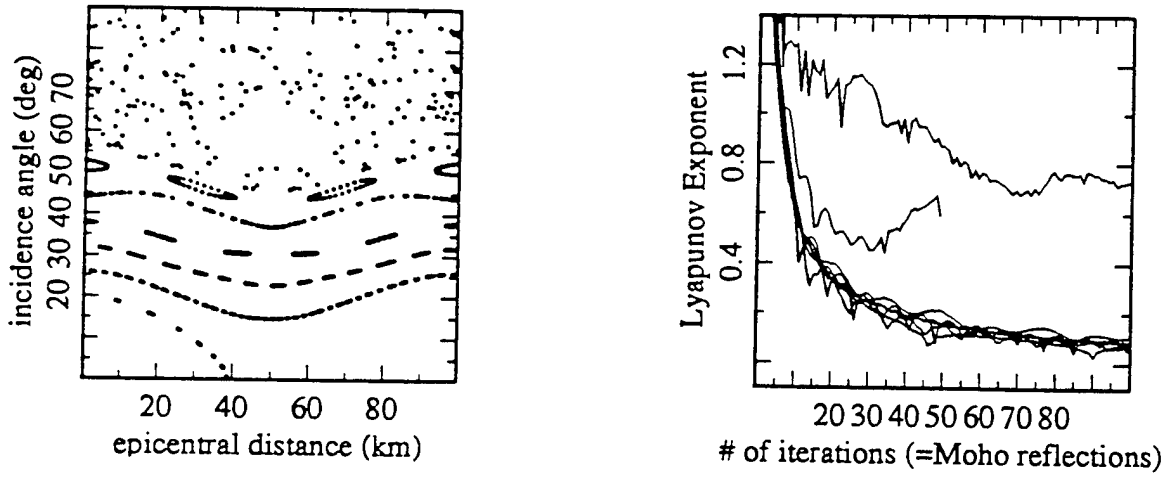

Figure 3. Phase space plots (left) and Lyapunov exponents (right) for 9 rays.

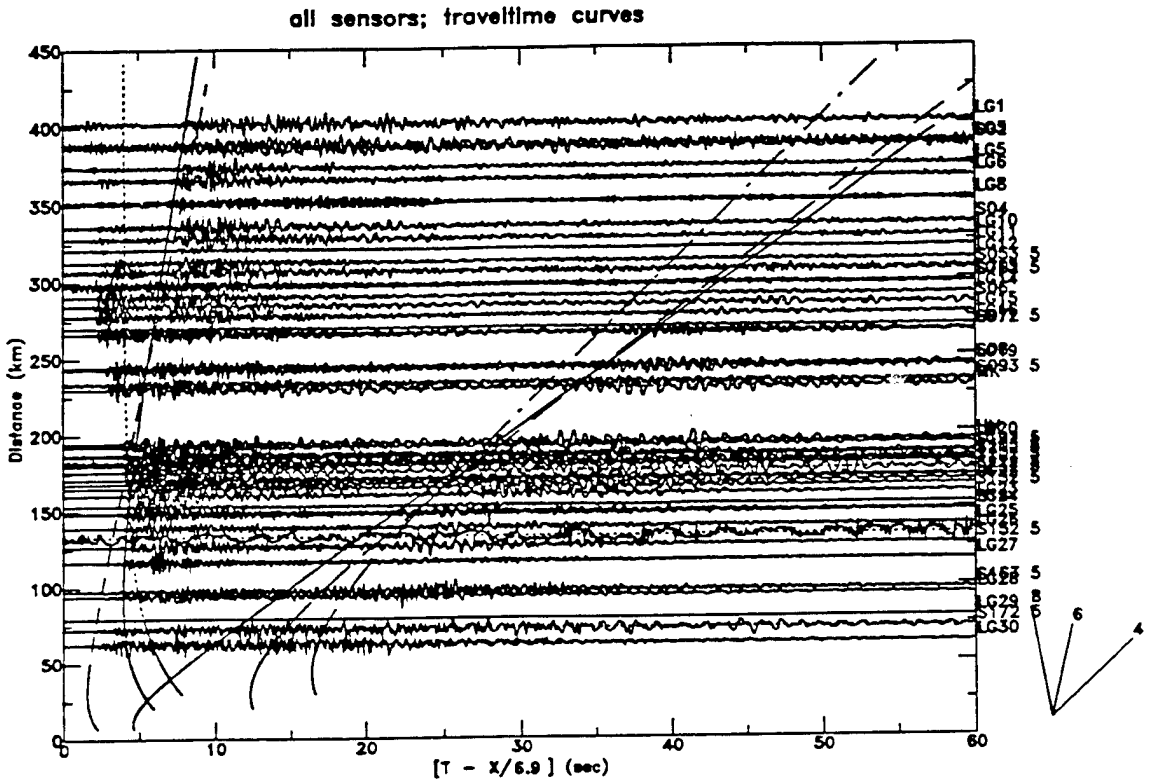

Figure 4. NPE data from the Nevada Test Site. The reduction velocity is 6.9 km/s. Traveltimes of PmP, SmS and midcrustal multiples are shown. Lg arrives after SmS.

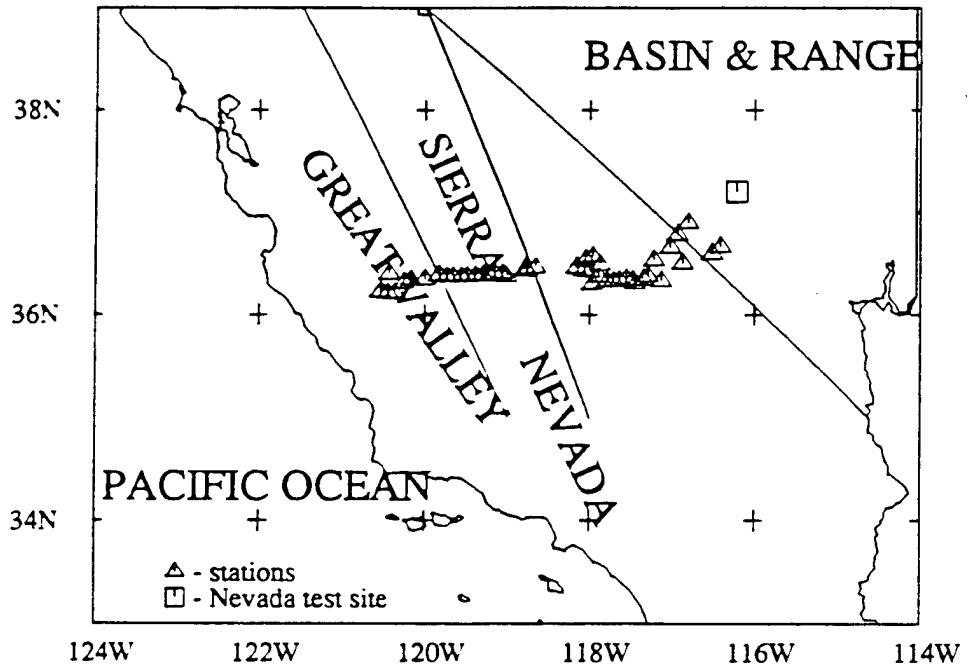

Figure 5. Source and station locations for the data shown in figure 4. Also indicated are the major tectonic provinces of the area.

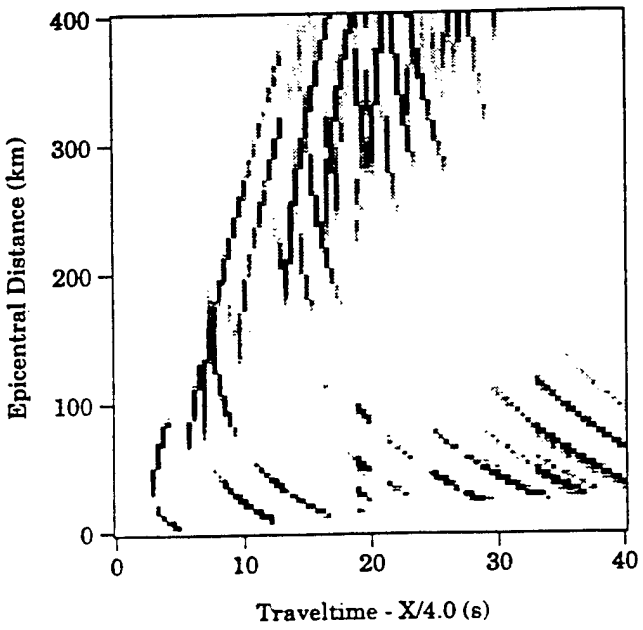

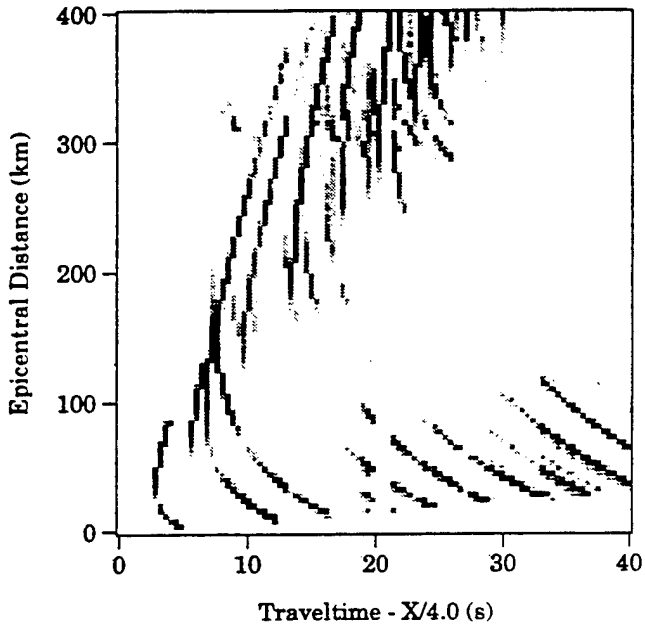

Figure 6a (left) and figure 6b (right). Ray density plots of Lg. The model corresponding to figure 6a is flat, the model corresponding to figure 6b has a bump in the Moho of 10 km and a wavelength of 100 km.

Figure 6c (left) and figure 6d (right). Same as figure 6b, with undulations of the midcrustal interfaces added (figure 6c) and random undulations (figure 6d).